UCRL-JRNL-203763

LX-17 Corner-Turning and Reactive Flow Failure

P. C. Souers, H. Andreski, C. F. Cook III, R. Garza, R. Pastrone, D. Phillips, F. Roeske, P. Vitello and J. D. Molitoris

March 12, 2004

Propellants, Explosives, Pyrotechnics

Updated October 14, 2003

LX-17 Corner-Turning and Reactive Flow Failure

P. Clark Souers*, Henry G. Andreski, Charles F. Cook III, Raul Garza, Ron Pastrone, Dan Phillips, Frank Roeske, Peter Vitello and John D. Molitoris

Energetic Materials Center, Lawrence Livermore National Laboratory, Livermore, CA USA 94550

*Corresponding author: e-mail: souers1@llnl.gov

Abstract

We have performed a series of highly-instrumented experiments examining corner-turning of detonation. A TATB booster is inset 15 mm into LX-17 (92.5% TATB, 7.5% kel-F) so that the detonation must turn a right angle around an air well. An optical pin located at the edge of the TATB gives the start time of the corner-turn. The breakout time on the side and back edges is measured with streak cameras. Three high-resolution X-ray images were taken on each experiment to examine the details of the detonation. We have concluded that the detonation cannot turn the corner and subsequently fails, but the shock wave continues to propagate in the unreacted explosive, leaving behind a dead zone. The detonation front farther out from the corner slowly turns and eventually reaches the air well edge 180^{o} from its original direction. The dead zone is stable and persists 7.7 μs after the corner-turn, although it has drifted into the original air well area. Our regular reactive flow computer models sometimes show temporary failure but they recover quickly and are unable to model the dead zones. We present a failure model that cuts off the reaction rate below certain detonation velocities and reproduces the qualitative features of the corner-turning failure.

Keywords: dead zone, corner-turning, X-ray, failure, reactive flow

1 Introduction

LX-17 (92.5 % TATB/7.5% kel-F 800) and PBX 9502 (95 and 5% respectively) have been much studied and are slightly non-ideal. Cox and Campbell studied the ability of 1.88-1.89 g/cm^3 PBX 9502 to turn corners using a long, cylindrical straight section that suddenly changes into a much wider cylinder, which has a slice taken out of one side. A streak camera sweeps the slice and from the two-dimensional picture, the dead zone size and shape is derived.[1] They concluded that the explosive had a 17 mm corner-turning radius, and that the explosive inside this radius did not detonate. The Cox/Campbell geometry has since been refined into a test by Manfred Held,[2,3] who used the term "dead zone" for the unreacted explosive.

The detonation of LX-17 ribs were also studied in the 1980's.[4,5] These were square sections of explosive that gently turned a 90^{o}-curve with the inner surface being marked with pins. The inner surface detonation velocity of 6.9-7.1 mm/μs was lower than any overall value found in ratesticks, but the minimum inner radius of 63.5 mm was so large than detonation apparently occurred everywhere. For a small-enough radius, failure should occur on the inner edge with the detonation successfully

turning the corner at some larger radius. Such corner turning radii of 9 to 26 mm was seen by Cox and Campbell for PBX 9502 in their double cylinder geometry.[1]

The Los Alamos flash X-ray facility PHERMEX came into being a generation ago and was used to look at detonation fronts [6,7] and even corner-turning[8]. The proton radiograph facility LANSCE at Los Alamos is the modern version,[9] which is being used to examine detonating high explosives.[10] Eric Ferm, et. al. repeated the Campbell/Held PBX 9502 geometry;[11] they saw the corner-turn average wave velocity drop to 3.3 mm/μs and assigned this to detonation failure. The burned product/dead zone front by contrast moved around the corner at only 0.9 mm/μs. The space in between these two fronts is the dead zone, and they noted that it lasted at least 6 μs after the turn. Straight ahead, the detonation velocity moved at normal speed. Finally, the DSD computer model that was tried did not model failure, and the need for a separate failure package in the model was noted.

A study of the two LLNL models Ignition & Growth and JWL++ showed that failure in ratesticks could not be simulated using the normal detonation settings of the parameters.[12] An increase of the pressure exponent, b_1, to larger values does give calculated failure which simulates actual failure but usually changes the size (diameter) effect curve to the wrong shape. Moreover, the failed detonation will recover with time. Operating the model near failure often produces instabilities as well. In this work, we shall show an empirical model that turns off permanently as the detonation turns the corner.

2 Experimental

The geometry of the ambient CTX experiment is shown schematically in **Figure 1**. The part is cylindrical with the axis of the revolution being the Z-axis (vertical) as indicated in the figure. A hemispherical detonator initiates the 1.80 g/cc TATB booster of radius 19.05 mm, which in turn initiates the main charge of LX-17. The crystal pin at the lower left indicates the basic straight-ahead performance; an optical pin tells when the detonation starts to leave the booster and turn the corner. Above the TATB booster is a cylindrical air well of radius 19.05 mm and length 15 mm, which defines the corner of interest. The length from the detonator to the bottom of the LX-17 part is 40.45 mm. Two radii of cylinders were used. The thick-wall version has a 44.45 mm radius so that the LX-17 extends 25.4 mm beyond the edge of the TATB. The thin-wall version has a 31.75 mm radius so that the LX-17 extends 12.7 mm beyond the edge of the TATB. Figure 1 is set so that the origin is at the point of the corner-turn rather than the axis of symmetry. The Z-axis is positive for corner-turning and negative for straight-ahead motion of the front.

The diagnostics used on this experiment included streak cameras which measured shock break-out on the surface of the explosive part, an optical pin for absolute timing, time sequence x-ray imaging to

examine the details of the detonation corner-turning, and a crystal pin for cross timing purposes. A short description of these diagnostics as applied to this experiment follows.

The main streak diagnostics looked at the top and sides in Figure 1. Poly-methyl-methacrylate flasher blocks were mounted on the edge such that 0.076 mm gaps existed between the LX-17 and the plastic. When the detonation waves break out on these surfaces, a flash of light occurs in the gap and is imaged on the photocathodes of two electronic streak cameras located just outside the tank. The camera viewing the side edge of the sample had a 3.0 μsec window and the camera viewing the back edge had a 1.0 μsec window.

To determine the time interval between the arrival of the detonation wave in the TATB at the corner and the breakout time at the edges of the LX-17, we used an optical pin technique. A probe normally used for Fabry-Perot experiments was placed in the aluminum holder arm so that laser light from the probe impinged upon the corner of an aluminized mirror surface in intimate contact with the explosive. We monitored the laser pulse with a Hamamatsu s3071 photodetector with a 532 nm bandpass filter in front of it. When the detonation wave reached the corner, the mirror was destroyed and the return laser pulse reflection disappeared.

Modern X-ray systems have sub-millimeter spot size combined with high flux. Our equipment had greater than 30 milli-roentgens radiation dose per pulse at 1 m with 0.5 mm full-width-half-maximum spot size. The set-up used for these experiments consisted of three 450 KeV flash x-ray units set at angles of 11 to 15 degrees from each other about the axis of symmetry of the high-explosive charge as shown schematically in **Figure 2**. The X-rays are projected from point sources on the right of the figure to the image planes on the left with the explosive located on the object plain in the center. In the lower diagram, the explosive sits just as it does in Figure 1, with the air well facing upward. Each X-ray unit projected a distinct non-overlapping image onto a common film pack. Magnifications from the three projections varied from 1.34 to 1.35. The temporal resolution was 25 ns as defined by the flash duration and was constant for all shots. The spatial resolution varied from shot to shot, but was typically in the range of 0.1 mm to 0.5 mm. As each of the three units could be independently triggered on a given shot, a time sequence could be obtained for the same shot/experiment. The diagnostic was heavily collimated to insure absolutely no cross-projections between the three X-ray channels. Each channel projected a well defined region of the object plane to the image plane with full image separation as illustrated in Figure 2 below. To confirm this, source intensity was compared vertically across the image sets. Vertical lineouts taken from these images have the same slope at the same image location.

The contrast was optimized primarily by adjusting the high-voltage of the diagnostic. Multi-plane film pack assemblies allowed a range of imaging sensitivities for each shot. As the high-explosive detonated in these shots was uncased, there was minimal fragmentation to possibly damage the film pack. Therefore,

we did not have to use heavy or complex shielding to protect either the x-ray heads or the film packs. We were able to use minimal shielding to mitigate the effects of blast and focus on minimizing background with absorbers to further optimize the contrast ratio.

Finally, to monitor the arrival of the detonation wave at the LX-17 surface on the cylindrical axis directly in line with the initiation point we placed a crystal pin detector at that point and recorded the results on a digitizing scope. This gave us a clear timing fiducial in the experiments. We monitored the current start to the detonator, the bridgewire burst time, the optical pin time, the crystal pin time, the time of firing of all three X-ray heads and an optical marker signal for the streak cameras on digitizing scopes. This gave us the cross-timing references to tie all of the data together.

3 Results

The distance from the edge of the TATB booster edge to the on-axis electrical pin was 21.36 mm. The average time difference between the optical pin and the electrical pin was 2.84 $\pm$ 0.02 μs. Now we compare the times on the edge of the TATB booster near the free edge, where the optical pin is, with the edge straight down from the detonator on the Z-axis. We estimate a 0.04 μs delay at the optical pin caused by the slower detonation velocity along the free edge at the bottom of the sir well. The result of four shots was 7.64 $\pm$ 0.06 mm/μs for the straight-ahead detonation velocity, in good agreement with cylinder results for LX-17.

Figure 3 shows the X-ray result at 2.48 μs after the optical pin. We are focusing on the corner-turn region indicated by the box in Figure 1. The straight-ahead detonation front is seen as the circular curve at the lower right. Going around the corner, however, the light-gray dead zone occupies the space near the booster. We might imagine that the top of the dead zone is the shock wave moving through unreacted explosive and the bottom is the detonation front, which has stalled. **Figure 4** shows the result at 7.74 μs. The detonation fronts have long since reached the edges and the rarefaction wave has reflected back. Yet the dead zone is still there and is being pushed into the empty air well by the gas products at the right.

We first consider the streak camera results, which are listed in **Table 1**. In terms of Figure 1, the direction runs upward along the right-hand edge from the bottom, then turns left across the top. This means we begin with the detonation propagating straight ahead and move progressively into the dead zone region. We use the times to calculate an average wave velocity from the edge of the TATB booster to the breakout point assuming constant velocity and a 0.04 μs lag for the pin behind the rest of the TATB edge. For large negative axial distances, we get the 7.6 mm/μs straight-ahead detonation velocity we expect in LX-17. As the axial Z values become more positive, the velocity decreases and failure occurs at some point. At the

farthest dead zone point, the velocity is only 3.5 mm/μs and this is the first reason for believing that detonation failure has occurred going around the corner. Using this wave velocity in the unreacted Hugoniot of LX-17 of[13]

$$U_s = 2.5 + 2.1u_p\,, \tag{1}$$

where the particle velocity, u_p, is 0.48 mm/μs and the pressure of 3 GPa is about 1/10th the detonation pressure.

Next we find the boundaries of the dead zones from the X-ray images. We obtain these boundaries by a combination of direct image analysis (where the dead zone is mapped directly from the image data) and the use of vertical line-outs (described below) to quantify the extent of the dead zone. In this latter technique, X-ray transmission intensity as a function of vertical distance for a fixed radius is extracted from the image and plotted. Clearly, this translates to density of the object being imaged and the discussion which follows is in terms of density. To decrease statistical fluctuations and noise, we use a wide line-out technique where several columns of pixels from the digitized image are averaged over. This averaging is consistent with the worst case spatial resolution of the X-ray diagnostic and usually fixed at the width of pixels equal to 0.5 mm. **Table 2**, therefore, lists the average (with some extrapolations) plus inner and outer estimated boundaries of the dead zone for both thin and thick-wall parts at the listed pin times. Only data for positive radial distances (to the right of the air well) are given, although both sides in the pictures have been averaged. Data is taken in the air well but not used here because of the difficulty of determining whether it is connected to the detonation corner-turning to the right or is a projection of the process seen straight through. We are presently working on density conversion and deconvolution techniques to remove the three-dimensional projection aspects of the X-ray data, but that work is not reported here. The asterisk in the table indicates the farthest right extent of that line. A code calculation would be considered successful if the density plot of the dead zone fell inside these markers. The times up to 2 μs look the same regardless of the part size. So all the data in Table 2 falls into the same time sequence except for the last "thin, 2.6 μs". Here, at 2.6 μs in the thin wall part, the straight-ahead shock wave has hit the edge and the rarefaction wave has pushed the dead zone upward as seen in **Figure 5**. The dead zone for the thick wall part, where no wall interaction has occurred, lies slightly below.

A set of thick wall dead zone boundaries are shown in **Figure 6**. The dead zones in the thick wall part expand outward and upward with time, reaching a maximum size at 3 μs. The shock wave reaches the upper edge at 3.5 μs. At longer times, the dead zones slowly contract but persist. The flat front on the top of the dead zone is moving at about 4 $\pm$ 1 mm/μs, in agreement with the streak camera and representative of a shock wave in unreacted explosive. The lower edge of the dead zone is the

boundary where burnt explosive is pushing upward so that it moves at about 0.5 mm/μs. The far right edge of the dead zone expands at 6 mm/μs up to 1.9 μs, then slows to 1.5 mm/μs from 1.9 to 3.0 μs. At late times, the rarefaction is pushing to the left and the dead zone boundary is retreating at about 1 to 1.5 mm/μs.

Also important for modeling is the information on the free detonation front, ie. that part expanding to the lower left and right in the figures. The coordinates at four times are listed in **Table 3**. The error in averaging both sides of each picture is about ±0.3 mm.

Figure 7 shows the film densitometer vertical lineouts across the thick-wall part at 2.48 μs. The down direction represents increasing density so that the trace has a tilt going the wrong way. That is because the top part of the figure is the unreacted explosive at 1.90 g/cc while the bottom is product gas at low density. The best we can do is to consider the troughs of the dead zones by themselves. The dead zone is really a half-torus wrapped around the air well, but it looks roughly like a half-ellipse in the picture with radii Z_o and R_o. The simplest function to consider is the distance through a slice of a sphere, which in the axial direction is

$$\sin\left[\cos^{-1}\left(\frac{Z}{Z_o}\right)\right] \tag{2}$$

with the same function existing radially in terms of R/R_o. This says that if the dead zone has a higher density than the surroundings, then the maximum X-ray absorption will occur next to the air well in the center of the circle. The intensity should drop rapidly as we move right to the edges of the dead zone. A fitting of Eq. 2 to the line-out data at 2.48 μs gives Z_o = 3.2-3.5 mm and R_o = 12 mm in agreement with the dimensions obtained by measuring the edges.

4 Code Results

We are using JWL++, a simple one-rate reactive flow model with the rate term

$$\frac{dF}{dt} = G_1 (P+Q)^{b1} (1-F). \tag{3}$$

where F is the burn fraction, P the pressure, Q the artificial viscosity, G_1 the rate constant and b_1 the pressure exponent. This is a stripped-down version of Ignition & Growth designed for detonation only. It shows simply the properties of pressure-dependent reactive flow models. The edge of convergence,

where the detonation velocity first behaves, is 4 zones/mm and we run at 4 and 8 zones/mm. The model is running in a 2-dimensional CALE-type arbitrary Lagrangian-Eulerian (ALE) hydrocode.

In JWL++, we have generally set $G_1 = 1.5\ (\mu s \cdot GPa)^{-1}$ because the $b_1 = 1$ setting has proved to be stable when used for many explosives. One way to make the model fail is to move up b_1 to just under 3. This high-b_1 approach shows a transient dead zone, but then the detonation recovers and the dead zone disappears. We also tried this with Ignition and Growth, which fails at $b_1 \approx 2$ because of the presence of an F term in the rate. Both show only temporary failure with subsequent reignition of the detonation.

We want to add detonation failure while keeping the model stable. In order to describe the observed dead zones in PBX 9502 with corner-turning, we define the failure parameter, k

$$k = [(u_{px} - u_{px}^{o})^2 + (u_{py} - u_{py}^{o})^2]^{1/2} + C \tag{4}$$

where u_p are particle velocities in the x and y directions and C is the sound speed. This is defined in each zone on every cycle and is a measure of the detonation velocity, albeit without actually calculating the distance moved per unit time. In each zone, we compare this value to the failure velocity, k_o, and either turn on the full rate constant or set it to zero:

$$\begin{aligned} &\text{if } k > k_O, \text{use } G_1 \\ &\text{if } k < k_O, \quad G_1 = 0 \end{aligned} \tag{5}$$

We also require as usual a pressure turn-on greater than 1 GPa. The presence of the undetonated reference frame velocities makes this quantity Lorentz-invariant; clearly, in our problem, both u_{px}^{o} and u_{py}^{o} are zero. Eq. 5 is an empirical way of requiring that a simulation of the detonation velocity reach a certain value for detonation to occur and it creates dead zones that do not turn on again. The cutoff value k_o is found by fitting the break-out times to the streak camera data.

Figure 8 shows the measured thick-wall streak camera data in times from the optical pin. The R-axis is the same used in Table 1, going up the right-hand edge and around the corner going left along the top, so we move from straight-ahead behavior to ever-deeper failure. It is important that a model fit both sides of this figure at once. The data (squares) and code runs (full and dashed lines) are shown. We find that agreement is obtained if we use $b_1 = 1$, $G_1 = 1.50\ (\mu s \cdot GPa)^{-1}$ at 4 zones/mm with $k_o = 7.93$ mm/μs but we get unacceptable results if $k_o = 0$ is used.

In **Figure 9**, we compare the edges of the dead zone (full lines) with the code (dashed) at 4 zones/mm. Agreement is qualitatively good in showing the dead zone to persist and to drift upward and to the left with time. At 7.7 μs, the dead zone has entered the original well region and the picture appears to show a stronger effect to the left as well.

We next consider the details of the calculated dead zone in the model at 2.48 μs with 8 zones/mm as shown in the density plot of **Figure 10**. The untouched explosive lies at the top with a density of 1.90 g/cc. The burned products lie at the bottom, all with densities less than 1.90. The dead zone, which is compressed but not burned, has a higher density with the density increasing from 2.0 to 2.4 g/cm^3 as we move radially out to the edge of the detonation front. At present, we cannot extract a density from our data. The pressure where the detonation front intersects the dead zone is about 10 GPa. The dead zone itself is at about 2-6 GPa with the pressure falling to zero near the air well. The density gradient seen here cannot be verified from the data. By 3.5 μs, the detonation front taking the long way around on the right appears. By 4.0 μs, it has reached the top surface and is moving at a 45^o angle toward the remaining unburned material near the top edge by the air well (Z = 0, R = 15). By 4.5 μs, the front has wrapped around the dead zone and isolated it totally. By 7.71 μs, an island of 2.0 g/cc remains. At 15.7 μs in the model, a smaller island of 2.0 g/cc is still seen, but the dead zone's right hand radial boundary has been pushed farther to the left to –28 mm .

We return to a consideration of our failure model. In going from 4 to 8 zones/mm, the cutoff k_o changes from 7.93 to 7.65 mm/μs. We had hoped that the failure model would not interfere with the rest of the reactive flow, but this is not so. The effect of using it is to weaken the rate constant, which causes the detonation velocity at small radii to droop down too much. We have mentioned that raising b_1 will weaken the model until it fails,**[12]** and we have found that this mechanism is the same as the one in our failure model. If we run with $b_1 = 1$, $G_1 = 1.5$ $(\mu s \cdot GPa)^{-1}$, the model fails in a ratestick between a 3 and 4 mm radius for $k_o = 7.93$ mm/μs. In going to $b_1 = 2.8$, $G_1 = 0.0025$ $(\mu s \cdot GPa^{2.8})^{-1}$, it fails at $k_o = 6.50$ mm/μs. Less k_o failure is needed because a high-b_1 model contains partial failure. Both show identical size effect curves which are too much concave-down. What makes the failure model different is that it stays off after the reaction stops, whereas the high-b_1 model falters but recovers.

We also split Eq. 4 into its two components and tried to induce failure first with $[(u_{px} - u_{px}^o)^2 + (u_{py} - u_{py}^o)^2]^{1/2}$ by itself and then with C by itself. We found that both cause a ragged dead zone to form just beyond the booster in the direct path, ie. the detonation does not turn the

corner at all. We see then that it takes both components in Eq. 4 together to obtain a dead zone in the right place.

4. Discussion

The failure model used here is entirely empirical. We now consider the data taken by Manfred Held before proton and X-ray radiography using the Campbell two-cylinder geometry.[2,3] The detonation ran up a narrow ratestick which suddenly expanded into a wide one, thereby forcing the detonation to try to turn the corner. A slice was made in the side of the broad ratestick and a streak camera measured the breakout so that all the data could be had from one shot. In **Figure 11**, we show it with the same labeled axes we use with our geometry. The detonation moves left to right in the R-direction (even though this is axial in the two-cylinder geometry). The corner-turn is a left turn going upwards in the Z-direction.

The dead zones are regions at the upper left. Held's PBX 9502 dead zone has a different shape than our X-ray LX-17 dead zone, partly because his data is taken at different times and ours at one time. Only one point exists for ideal tetryl and 95% RDX so that they appear to have small dead zones. It is a surprise to find that Comp B (65% RDX/TNT) has an even larger dead zone than PBX 9502. This would appear to violate the ideality sequence we are looking for, but perhaps the corner-turning shock wave liquefies the TNT and renders it less ideal. More data on this issue is needed.

5 Conclusions

X-ray transmission proves to be an excellent technique for studying detonation failure resulting from tight corner turns. Future work will concentrate on the effect of confinement in the air well and the results at colder temperatures.

Acknowledgements

We would like to thank Ernie Urquidez and Rich Villfana for the firing tank, Tom Crabtree for optical pin recording, and Gary Steinhour for electrical firing. For additional support of the experiment, we appreciate the work of Barry Levine and Steve Mudge for mechanical engineering, Gurcharn Dhillon for X-ray and mechanical, Michael R. Martin for operations, and Rick Palmer and Gary Steinhour for electronics. Sabrina Fletcher did an excellent job on experiment documentation and reduction/analysis of the X-Ray data. We acknowledge and appreciate many useful discussions with Maurice Aufderheide. Finally we acknowledge and appreciate the support of Jon Maienschein and John F. Alvarez for this research. This work was performed under the auspices of the U.S. Department of Energy by the University of California, Lawrence Livermore National Laboratory under Contract No. W-7405-Eng-48.

References

1. M. Cox and A. W. Campbell, Corner-Turning in TATB, *Proceedings Seventh Symposium (International) on Detonation,* Annapolis, MD, June 16-19, **1981**, pp. 624-633.

2. M. Held, Corner-Turning Distance and Retonation Radius, *Propellants, Explosives, Pyrotechnics* **1989***, 14*, 153-161.

3. M. Held, Corner Turning Research Test, *Propellants, Explosives, Pyrotechnics* **1996***, 21*, 177-180.

4. P. C. Souers, S. R. Anderson, B. Hayes, J. Lyle, E. L. Lee, S. M. McGuire and C. M. Tarver, Corner Turning Rib Tests on LX-17, *Propellants, Explosives, Pyrotechnics* **1998***, 23*, 1-8.

5. P. Clark Souers, Estella McGuire, Raul Garza, Frank Roeske and Peter Vitello, The Diverging Sphere and the Rib in Prompt Detonation, *Proceedings Twelfth International Detonation Symposium,* San Diego, CA, August 11-16, **2002**, to be published.

6. D. Venable and T. J. Boyd, Jr., Phermex Applications to Studies of Detonation Waves and Shock Waves, *Proceedings Fourth Symposium (International) on Detonation*, White Oak, MD, October 12-15, **1965,** pp. 639-647.

7. W. C. Rivard, D. Venable, W. Fickett and W. C. Davis, Flash X-Ray Observation of Marked Mass Points in Explosive Products, *Proceedings Fifth Symposium (International) on Detonation*, Pasadena, CA, August 18-21, **1970**, pp. 3-11.

8. C. L. Mader, Two Dimensional Homogenous and Heterogeneous Detonation Wave Propagation, *Proceedings Sixth Symposium (International) on Detonation,* Coronado, CA, August 24-27, **1976**, pp. 405-413.

9. J. D. Zumbro, K. J. Adams, K. R. Alrick, J. F. Amann, J. G. Boissevain, M. L. Crow, S. B. Cushing, D. Clark, J. C. Eddleman, C. J. Espinoza, E. N. Ferm, T. T. Fife, R. A. Gallegos, J. Gomez, N. T. Gray, G. E. Hogan, V. H. Holmes, S. A. Jramillo, N. S. P. King, J. N. Knudsen, R. K. London, R. P. Lopez, J. B. McClelland, F. E. Merrill, K. B. Morley, C. L. Morris, P. D. Pazuchanics, C. Pillai, C. M. Riedel, J. S. Sarracino, A. Saunders, H. L. Stacy, B. E. Takala, O. Trujillo, H. E. Tucker, M. D. Wilke, G. J. Yates, H.-J. Ziock, S. Balzer, P. A. Flores and R. T. Thompson, Proton Radiography of the Detonation Front in HE Sytsems, *Eleventh International Detonation Symposium,* Snowmass Village, CO, August 31-September 4, **1998**, pp. 54-65.

10. C. L. Mader, J. D. Zumbro and E. N. Ferm, Proton Radiographic and Numerical Modeling of Colliding, Diverging PBX 9502 Detonations, *12th International Detonation Symposium*, August 11-16, **2002**, San Diego, CA, to be published.

11. E. N. Ferm, C. L. Morris, J. P. Quintana, P. Pazuchanic, H. Stacy, J. D. Zumbro, G. Hogan and N. King, Proton Radiography Examination of Unburned Regions in PBX 9502 Corner Turning Experiments, 12th *American Physical Society Topical Conference on Shock Compression in Condensed Matter*, Atlanta, GA, June 24-29, **2001**, pp. 966-969. We would like to thank Eric Ferm of Los Alamos National Laboratory for personal communications in 2002-2003.

12. P. C.Souers, R. Garza and P. Vitello, Ignition & Growth and JWL++ Detonation Models in Coarse Zones, *Propellants, Explosives, Pyrotechnics* **2002***, 27*, 62-71.

13. D. C. Dallman and Jerry Wackerle, "Temperature-Dependent Shock Inititation of TATB-Based Explosives," *Proceedings Tenth Symposium (International) on Detonation,* Boston, MA, July 12-16, **1993**, pp. 130-138.

Table 1. Measured pin times and average wave velocities from the streak camera measurements. The thick-wall data is at the top and the thin-wall at the bottom. In terms of Figure 1, the direction runs upward along the right-hand edge, then turns left across the top.

Radial Distance (mm)	Axial Distance (mm)	Pin Time (μs)	Average Wave Vel (mm/μs)
25.4	-30	4.54	7.61
25.4	-25	4.22	7.57
25.4	-20	3.92	7.58
25.4	-15	3.68	7.58
25.4	-10	3.52	7.53
25.4	-5	3.45	7.44
25.4	0	3.49	7.28
25.4	5	3.65	7.08
25.4	10	3.98	6.85
25.4	12.5	4.19	6.75
25.4	15	4.40	6.70
20.0	15	3.95	6.33
15.0	15	3.66	5.80
10.0	15	3.59	5.02
5.0	15	3.80	4.16
2.5	15	4.01	3.79
0.0	15	4.24	3.54
12.7	-30	3.23	7.62
12.7	-25	2.78	7.70
12.7	-20	2.41	7.65
12.7	-15	2.14	7.52
12.7	-10	1.91	7.45
12.7	-5	1.78	7.36
12.7	0	1.87	6.79
12.7	5	2.36	5.80
12.7	10	3.12	5.18
12.7	12.5	3.56	5.00
12.7	15	3.90	5.04
10.0	15	3.72	4.85
5.0	15	3.90	4.05
2.5	15	4.11	3.70
0.0	15	4.35	3.45

Table 2. Summary of positions of the measured dead zone edges. At a given radial setting, R, we give the average axial value, Z, plus the inner and outermost positions based on the errors of measurement. All the data falls into the same time sequence except for the last "thin, 2.6 μs" section which has rarefaction effects. The axial distance is Z, the radial distance is R.

Wall/ Pin Time (μs)	R (mm)	ave Z (mm)	Outer Z (mm)	Inner Z (mm)	Wall/ Pin Time (μs)	R (mm)	ave Z (mm)	Outer Z (mm)	Inner Z (mm)
Thick,	0.0	0.04	-0.8	0.9	Thick,	0.0	2.19	1.8	2.6
0.86	2.0	-0.09	-0.9	0.7	3.00	5.0	3.04	2.6	3.5
	4.0	-0.15	-0.8	0.5		10.0	6.04	5.2	6.9

	5.2	0.80				12.0	10.65		
	4.0	1.81	2.4	1.2		10.0	11.38	11.7	11.1
	2.0	2.49	3.0	2.0		5.0	10.89	11.5	10.2
	0.0	2.60	2.9	2.3		0.0	11.81	12.6	11.1
Thin	0.0	1.18	0.6	1.7	Thick	0.0	3.85	3.4	4.3
1.25	4.0	0.99	0.6	1.3	6.11	2.0	3.89	3.3	4.5
	8.5	1.10				4.0	4.28	3.6	4.9
	8.0		1.8			6.0	5.05	4.3	5.8
	4.0	2.94	3.3	2.6		8.0		5.3	
	0.0	3.65	3.7	3.6		8.5	7.80		
Thin	0.0	1.78	1.4	2.2		8.0		11.2	
1.83	5.0	1.93	1.5	2.4		6.0	11.62	12.9	10.3
1.99	12.0		2.5			4.0	12.64	13.8	11.5
Thick	12.5	4.00				2.0	13.30	14.3	12.3
2.05	12.0		4.9			0.0	13.50	14.5	12.5
	10.0	5.30	5.7		Thick	0.0	4.93	4.0	5.9
	5.0	6.28	7.1	5.5	6.61,	2.0	5.23	4.2	6.3
	0.0	5.85	6.6	5.1	7.74	4.0	5.79	4.4	7.2
Thick	0.0	1.42	0.6	2.3		7.4	9.30		
2.48	5.0	1.72	0.9	2.5		8.0		10.6	
	10.0	3.16	1.4	4.9		6.0		12.7	
	11.0	5.80				4.0	13.24	14.0	12.5
	12.1		4.3			2.0	13.99	14.8	13.2
	11.0	5.80	7.5		Thin	0	2.25	1.9	2.6
	10.0	7.65	8.0	7.3	2.60,	5	2.45	2	2.9
	5.0	8.27	8.7	7.9	2.6	10	5.8	4.1	
	0	8.04	8.5	7.6		11	8		
						11.6		7.5	
						10.5			7.9
						10	9	10.7	
						5	9.3	10.3	8.3
						0	8.55	9.2	7.9

Table 3. Measured positions of the free detonation front as obtained from X-ray pictures. The error bars are roughly ±0.3 mm.

	R (mm)			
	Thick	Thin	Thick	Thick
Z (mm)	0.86 μs	1.25 μs	1.62 μs	2.48 μs
0	6.4	9.4	12.6	18.7
-5	6.0	10.2	12.3	19.0
-10	4.7	9.2	11.3	18.2
-20	-1.1	3.2	6.0	14.0

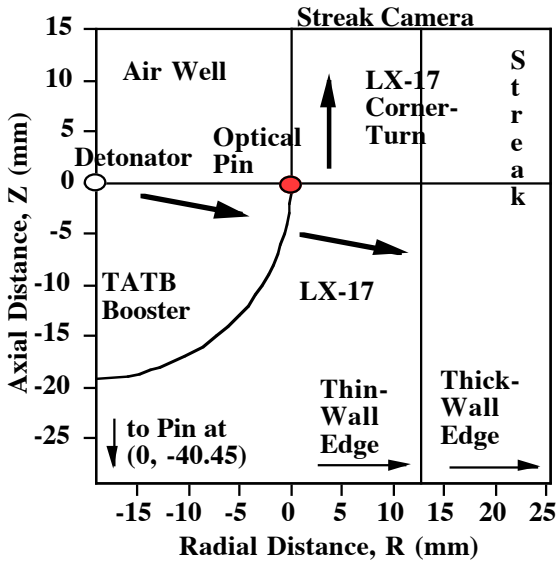

Figure 1. Schematic of the corner-turning geometry. The origin is the optical pin at the booster/air/LX-17 boundary. The thick-wall is 25.4 mm right from the optical pin; the thin wall is 12.7 mm.

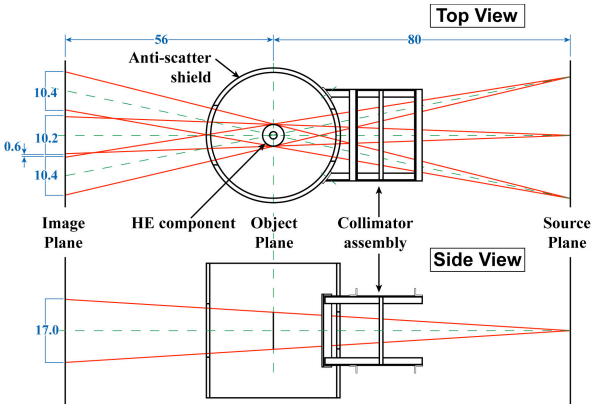

Figure 2. Schematic of the X-ray diagnostic geometry showing top and side views. The X-rays are projected from point sources on the right to the image plane on the left with the explosive sample being centered on the object plane in the middle. The collimation and shielding allowed no measurable cross-talk between the three X-ray channels.The image separation on the film pack assembly is about 15 mm.

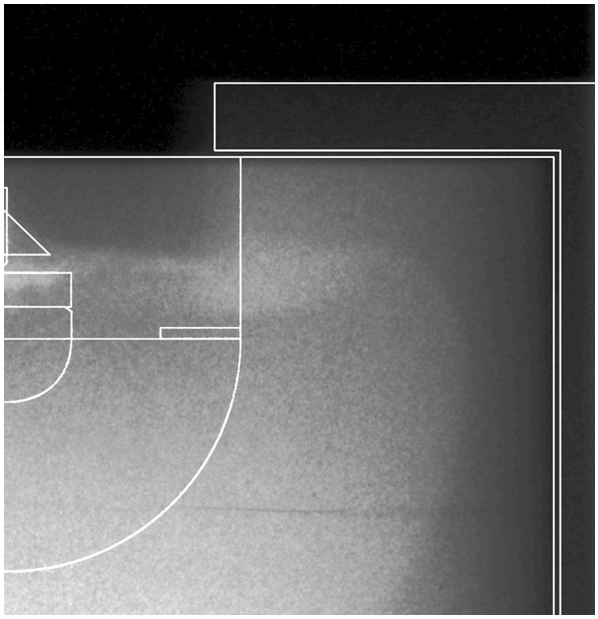

Figure 3. Thick-wall X-ray taken 2.48 μs after the optical pin. The picture has the geometry of Figure 1 with the initial features outlined in white. The detonation spreads left to right and turns upward around the corner. The oval at top center is the dead zone. The curve at the far right is the detonation front. At the very top is air.

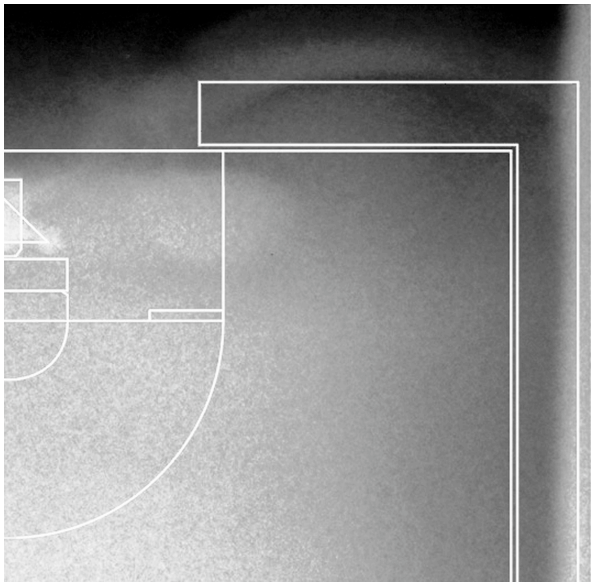

Figure 4. Thick-wall X-ray taken 7.74 μs after the optical pin. The dead zones at top center is still there and has drifted more left into the air well. The detonation front has long since passed.

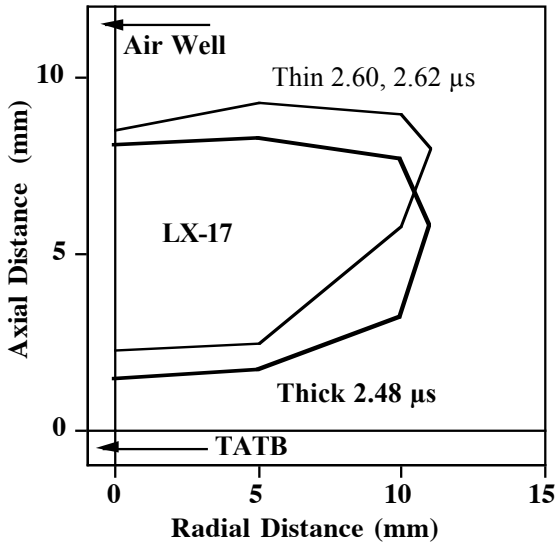

Figure 5. Average boundaries for the dead zones at 2.0-2.6 µs. The thin wall (light line) dead zone lies slightly higher than the thick wall (full line) because of the rarefaction wave off the edge. The origin is the optical pin at the booster/air/LX-17 boundary.

Figure 6. Average positions of the dead zone in the thick wall parts at various times. The times after passing e occurs at 3.0 µs. A shrinking but persistent dead zone i

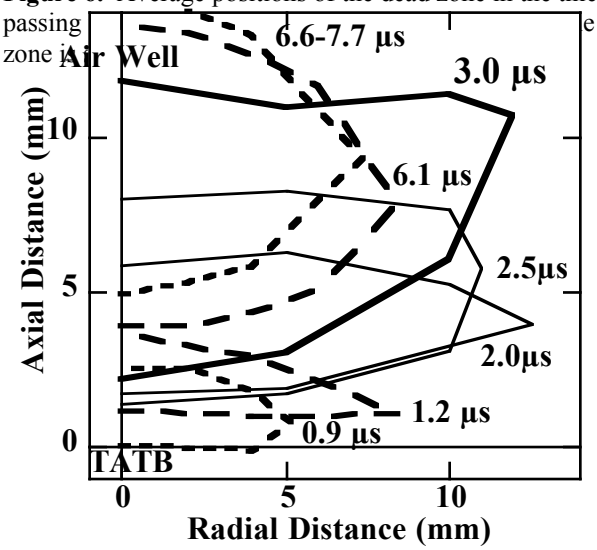

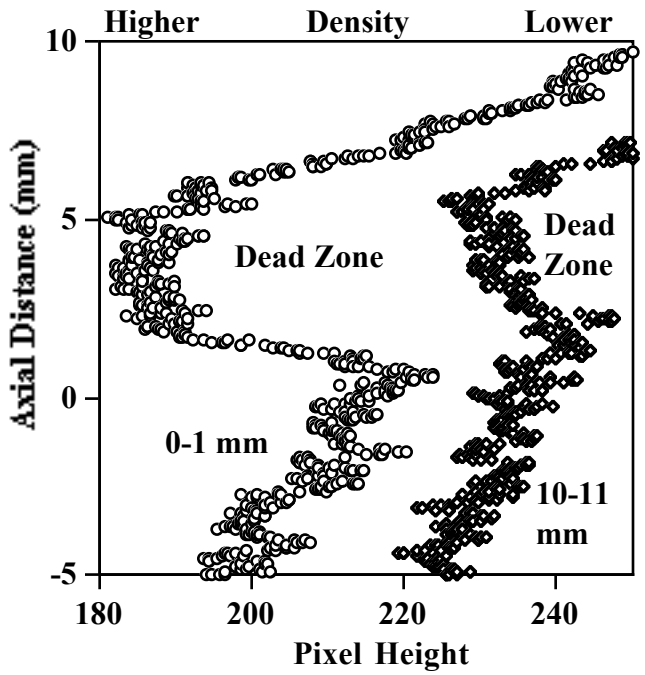

Figure 7. Measured vertical line-outs for a thick-wall sample at 2.48 μs. The radial distances from the air well edge are listed. The trough is the dead zone, which is larger near the air well than farther into the part.

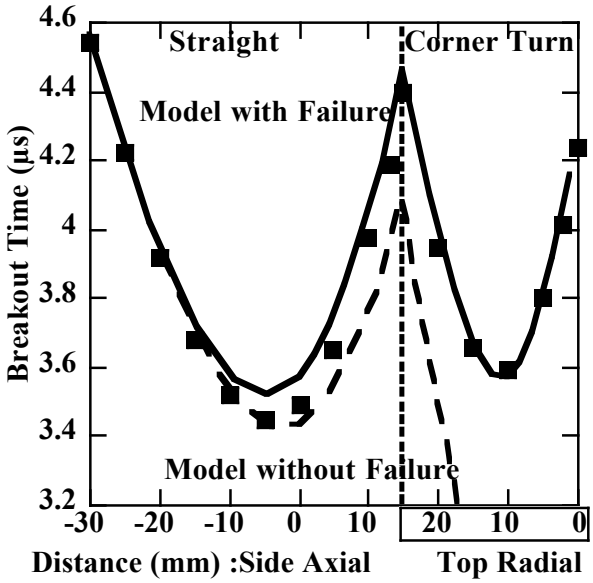

Figure 8. Streak camera pin times for the thick-wall geometry. The Z-axis runs vertically upward on the side, then turns left across the top (see Fig. 1). The straight-ahead section runs from –30 to 0 mm; on the right, the corner turn gets ever steeper. The data are the squares, the failure model is the full line and the no-failure model is the dashed line. Only the failure model works in the corner turn.

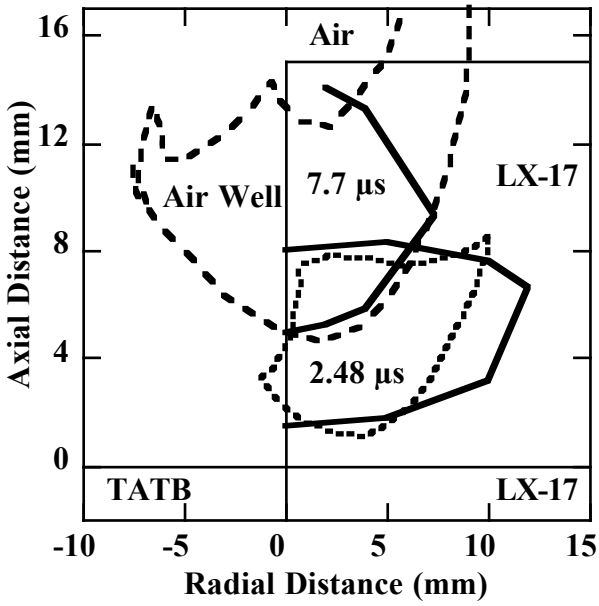

Figure 9. Comparison of the dead zone edges between the data (full lines) and the model (dashed) for the thick-wall part. With time, the dead zone has moved upward and to the left. The code predicts that the dead zone has entered the air well region at 7.7 μs.

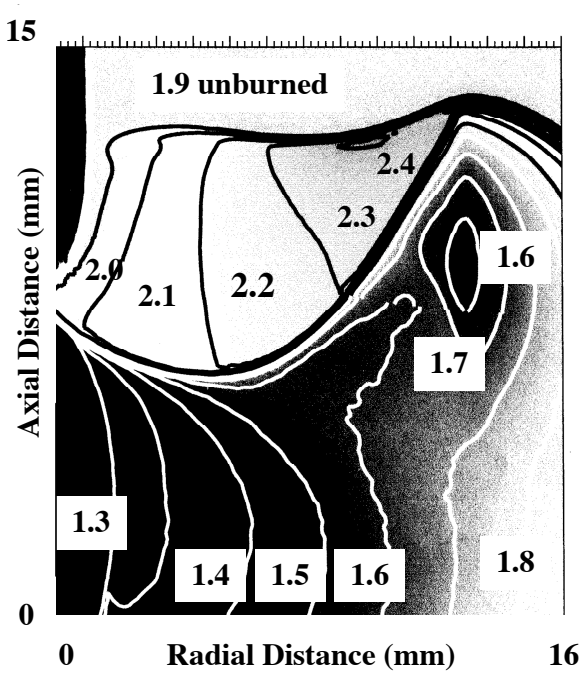

Figure 10. JWL++ code run at 8 zones/mm on the thick wall part at 2.48 μs pin time with $b_1 = 1$, $G_1 = 1.5$ showing the dead zone. The numbers are densities in g/cm^3. There is a density gradient extending from the end of the detonation front left to the air well.

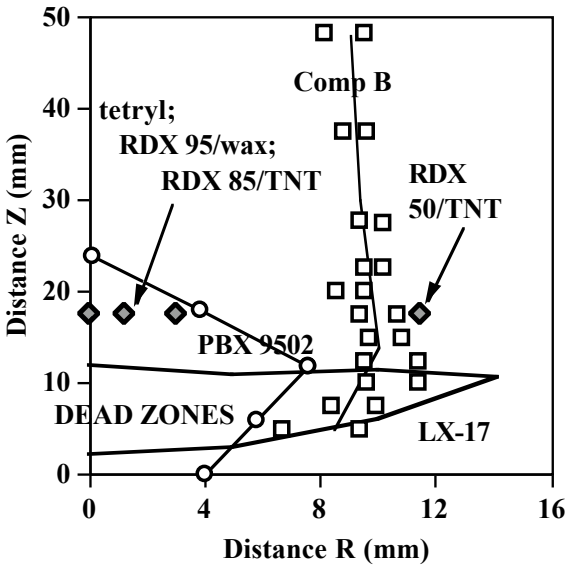

Figure 11. Corner-turning double-cylinder breakout data cast into our Figure 1 format for comparison. The dead zones are regions at the left defined by the lines. The PBX 9502 (circles) data is roughly in the same place as the LX-17 X-ray data (heavy line) taken in this paper. Comp B (squares) has a large dead zone. Only single points exist for four other explosives.